Interfacial delamination-induced unidirectional propagation of guided waves in multilayered media

Yanzheng Wang
Department of Civil Engineering, University of Siegen, Siegen, Germany

Zhengyang Li
Department of Civil Engineering, University of Siegen, Siegen, Germany

Mikhail V Golub(iD)
Institute for Mathematics, Mechanics and Informatics, Kuban State University, Krasnodar, Russia

Guoliang Huang
Department of Mechanical and Aerospace Engineering, University of Missouri, Columbia, MO, USA

Weiqiu Chen(iD)
Key Laboratory of Soft Machines and Smart Devices of Zhejiang Province, Hangzhou, China; Department of Engineering Mechanics, Zhejiang University, Hangzhou, China; Shenzhen Research Institute, Zhejiang University, Shenzhen, China

Chuanzeng Zhang
Department of Civil Engineering, University of Siegen, Siegen, Germany

Abstract
Unidirectional nonreciprocal wave propagation is an unprecedented phenomenon, which has attracted much research interest. Connecting a phononic crystal with an asymmetric structure to break the spatial inversion symmetry is a

Corresponding authors:
Weiqiu Chen, Department of Engineering Mechanics, Zhejiang University, Hangzhou 310027, China.
Email: chenwq@zju.edu.cn

Chuanzeng Zhang, Department of Civil Engineering, University of Siegen, Siegen 57068, Germany.
Email: c.zhang@uni-siegen.de

popular manner to realize this phenomenon using the wave mode transformation. In this paper, a new model is proposed based on a single periodic structure. The arrays of asymmetric and symmetric interfacial delaminations are intentionally introduced into the top and the bottom part of a stack of periodic elastic layers, respectively. So, the structural spatial inversion symmetry can be broken and the guided waves can pass through the whole structure only from the top side with the changed mode generated by the array of asymmetric interfacial delaminations. Thus, it is indispensable for the part of phononic crystal that the partial band-gaps of symmetric and antisymmetric guided waves have to be separated, which is the reason why we introduce the array of symmetric central or side interfacial delaminations into the stack of periodic elastic layers. The transmission spectra of the guided waves and the dispersion curves for the unit cell imposed by the Bloch–Floquet boundary condition are both calculated by the spectral element method. Then, the interfacial delamination-induced unidirectional propagation of guided waves in the finite stack of periodic elastic layers is numerically confirmed. This paper provides a new concept to control the waves propagating in phononic crystals via the insertion of some interfacial delaminations or cracks.

1. Introduction

The investigation on the acoustic/elastic waves propagating in periodic structures/materials has attracted considerable attention. Such structures are often called phononic crystals or acoustic/elastic metamaterials, which are well known for their outstanding capacity for the control of acoustic/elastic wave propagation. In addition, some unprecedented acoustic/elastic wave phenomena or novel acoustic wave devices can be realized through the artificial design of the unit cells within the periodic structures/materials, such as negative refraction [1,2], focusing [3], cloaking [4], wave filtering [5], waveguides [6], acoustic superlens [7] and demultiplexer [8].

In recent years, the investigation on the acoustic/elastic diode starts to thrive inspired by electric and optical diodes, which can realize the unidirectional nonreciprocal transmission of energy [9]. For most conventional materials, the principle of reciprocity is satisfied that waves will propagate symmetrically between the source and the receiver [10]. It has been proved that the unidirectional nonreciprocal acoustic/elastic wave propagation can be realized by breaking either the time reversal symmetry or the spatial inversion symmetry. Liang et al. [11,12] proposed a simple structure connecting a phononic crystal with a strongly nonlinear medium to break the time reversal symmetry. The waves incident from the side of the phononic crystal are blocked within the band-gap, while, the waves incident from the side of the nonlinear medium at the same frequency pass through the phononic crystal successfully. Actually, the transmitted waves are the higher harmonics generated by the fundamental waves in the nonlinear medium. The shortcoming for this model is that the unidirectional transmission is quite low due to the inherent low conversion efficiency in acoustic nonlinear activities [13]. Spatiotemporal periodic structures are also able to break the time reversal symmetry based on totally linear materials, whose material properties vary with time [14–16]. However, the fabrication and the practical operation for spatiotemporal periodic structures seem more complicated. To break the spatial inversion symmetry, a combined structure composed of a symmetric phononic crystal and an asymmetric structure was proposed [13,17,18]. It is known that the waves propagating in a finite thickness structure, called guided waves, have multi modes [19–24]. For example, there are three kinds of guided waves in an elastic layer, i.e., symmetric Lamb wave, antisymmetric Lamb wave, and SH wave, which can be transformed to each other by an asymmetric structure [25]. The wave with a specified mode excited from the side of the phononic crystal cannot propagate within the band-gap, while the same waves incident from the side of the asymmetric structure can do by changing its' mode. The spatial inversion symmetry can also be broken by the graded phononic crystals, in which the unidirectional wave propagation is possible due to the particular excitation way [26,27]. For example, the wave propagation is prohibited along the direction of the increasing material constants in the band-gap, while the same wave can propagate along the opposite direction due to the resonance. The limitation for graded phononic crystals is that the working frequency range is narrow
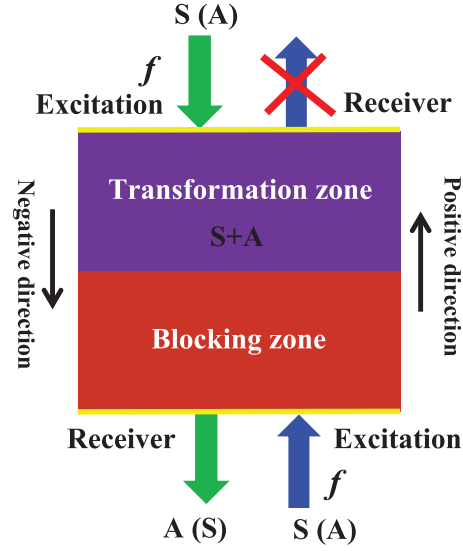
Figure 1. The conceptual illustration of unidirectional propagation of guided waves.
"S" and "A" represent the symmetric and the antisymmetric guided waves, respectively. The "transformation zone" denotes the zone where the wave mode transformation occurs, and the "blocking zone" can be used to block the guided waves with the specified mode in the band-gap. The whole structure is composed of a stack of periodic elastic layers (see Figure 2).
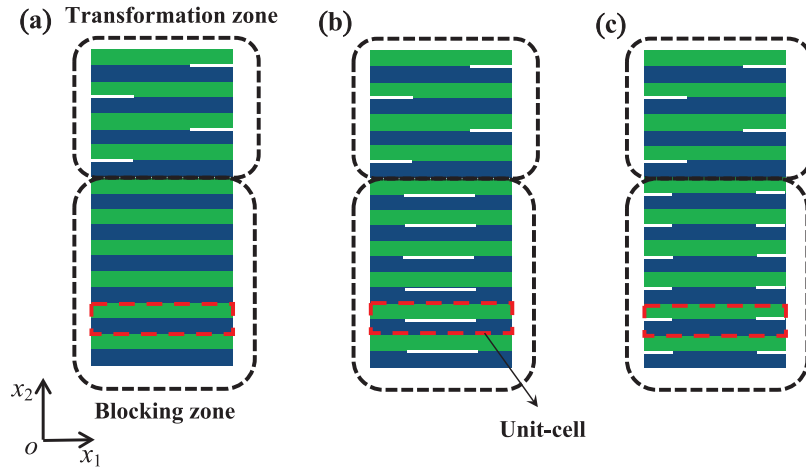

Figure 2. The schematic diagram of the stack of periodic elastic layers which enable the unidirectional propagation of guided waves for the blocking zone (a) without interfacial delamination, (b) with the array of symmetric central interfacial delaminations, and (c) with the array of symmetric side interfacial delaminations.

and the resonance frequency is much sensitive to the boundary conditions. It seems the challenge to design a desirable acoustic/elastic diode, which can gain wide engineering applications, still exists.

In this paper, the interfacial delaminations (or interfacial cracks) induced unidirectional propagation of guided waves is investigated. Instead of connecting a phononic crystal with an asymmetric structure, we simply insert an array of asymmetric interfacial delaminations into a stack of periodic elastic layers. The whole structure can be separated into two parts (see the conceptual illustration in Figure 1). The bottom part called the blocking zone is used to block the guided waves in the band-gaps. The top part called the transformation zone where the wave mode transformation occurs, which consists of an array of asymmetric interfacial delaminations (see Figure 2). Thus, the guided waves can transmit over the blocking zone with the changed mode.

It should be pointed out that whether there exist the separated partial band-gaps of guided waves is the key point for the blocking zone. However, the shortcoming of the stack of periodic elastic layers is that the partial band-gap of symmetric guided waves does not exist in the low frequency. To improve the efficiency of the present model, the array of symmetric (central or side) interfacial delaminations is inserted into the blocking zone (see Figure 2(b) or (c)), which can help us gain more band-gaps, especially the separated partial band-gaps [28]. The transmission spectra of the guided waves propagating in the finite stack of periodic elastic layers with interfacial delaminations and the dispersion curves for the corresponding unit cell imposed by Bloch–Floquet boundary conditions are both calculated by the spectral element method (SEM), which has been proven to be a more efficient numerical method than the conventional finite element method (FEM), especially for the high-frequency wave propagation problems [28,29]. The working frequencies can be uncovered through the partial band-gaps of guided waves propagating in the blocking zone. Then, the unidirectional propagation of symmetric (antisymmetric) guided waves in the finite stack of periodic elastic layers with the array of interfacial delaminations is numerically confirmed. Furthermore, the influences of the arrays of symmetric central and side interfacial delaminations on the unidirectional transmission are also taken into account. The proposed model may have potential applications in the field of wave propagation isolation and information processing. In addition, we pave an avenue to control the waves propagating in phononic crystals by intentionally introducing some interfacial delaminations or cracks.

This paper is composed of five main parts. Section 2 gives a detailed description of the proposed model. In section 3, the derivation of the SEM is presented. Section 4 shows the numerical results of the transmission spectra and the dispersion curves, and the corresponding discussions are also presented. In section 5, some concluding remarks are given.

2. Model description

The stack of periodic elastic layers is under consideration in a plane strain setting. The arrays of asymmetric and symmetric interfacial delaminations are both intentionally introduced to this structure to realize the unidirectional propagation of guided waves. There are only two wave mode shapes for the guided waves propagating in such structures, i.e., the symmetric wave mode and the antisymmetric wave mode with respect to the central line in the direction of x_2-axis. The array of asymmetric interfacial delaminations is inserted into the top part (i.e., the transformation zone, see Figure 2) to induce the wave mode transformation, in which the symmetric (antisymmetric) guided waves can be generated by the antisymmetric (symmetric) guided waves. The part containing the array of symmetric interfacial delaminations can be regarded as a new phononic crystal used to block the guided waves with the specified mode in the partial band-gap (see the array of the symmetric central interfacial delaminations in Figure 2(b) and the arrays of the symmetric side interfacial delaminations in Figure 2(c)).

The stack of 40 elastic layers is considered, which is composed of two different materials (M1 and M2) distributed periodically along the x_2-axis (see Figure 2). The two materials are selected as aluminum and epoxy, respectively. The mass density, Poisson's ratio and Young's modulus of aluminum and epoxy are set as $\rho^{(1)} = 2700$ kg/m^3, $\nu^{(1)} = 0.33$, $E^{(1)} = 70$ GPa, and $\rho^{(2)} = 850$ kg/m^3, $\nu^{(2)} = 0.45$, $E^{(2)} = 0.5$ GPa, respectively. In the following part, it is assumed that the blocking zone contains 26 elastic layers (13 unit cells) and the transformation zone contains 14 elastic layers. The width and height of each elastic layer are set as $w = 0.02$ m and $h_0 = 0.002$ m, respectively. The lengths of each central interfacial delamination and each side interfacial delamination in the blocking zone are 0.01 and 0.005 m, respectively. The length of each side interfacial delamination in the transformation zone is 0.005 m too.

The generalized equations of motion for the time-harmonic elastic waves propagating in a two-dimensional (2D) elastic medium are given by

$$\sigma_{ij,j} + b_i + \rho\omega^2 u_i = 0, \tag{1}$$

where $i = 1, 2$ and $j = 1, 2$, a comma in the subscript denotes the corresponding spatial derivative and the repeated subscripts imply the summation, ρ is the mass density, b_i represents the body force in the x_i-direction, and ω is the angular frequency. The components of the stress tensor σ_{ij} can be expressed by the displacement components u_i as

$$\sigma_{11} = \frac{E}{(1+\nu)(1-2\nu)}\left[(1-\nu)\frac{\partial u_1}{\partial x_1} + \nu\frac{\partial u_2}{\partial x_2}\right], \sigma_{12} = \frac{1}{2}\frac{E}{1+\nu}\left(\frac{\partial u_1}{\partial x_2} + \frac{\partial u_2}{\partial x_1}\right),$$

$$\sigma_{22} = \frac{E}{(1+\nu)(1-2\nu)}\left[\nu\frac{\partial u_1}{\partial x_1} + (1-\nu)\frac{\partial u_2}{\partial x_2}\right]. \tag{2}$$

The common time-harmonic factor $e^{-i\omega t}$ appearing in all physical quantities is neglected throughout this paper for the sake of brevity.

For the perfectly bonded elastic layers, the displacement and stress fields on the interface should be continuous, which can be described by

$$u_i^{(1)} = u_i^{(2)}, \sigma_{2i}^{(1)} = \sigma_{2i}^{(2)}, (i = 1, 2), \tag{3}$$

where the superscripts "1" and "2" in the brackets denote the two different materials M1 and M2, i.e., the aluminum and the epoxy, respectively. If there is an interfacial delamination between two neighboring layers, it is assumed that the two debonded surfaces do not interfere with each other. It means that the displacement fields are discontinuous and the stress-free boundary conditions are satisfied on the two faces of the delamination, which can be written as follows

$$\sigma_{22}^{(1)} = \sigma_{22}^{(2)} = 0, \sigma_{12}^{(1)} = \sigma_{12}^{(2)} = 0. \tag{4}$$

For a phononic crystal, any unit cell can be repeated by a translation vector $\mathbf{r} = r_1\mathbf{e}_1 + r_2\mathbf{e}_2$, where r_1 and r_2 are the constant multiple of the lengths of the unit cell in the x_1- and x_2-directions, respectively, and $\mathbf{e}_1$ and $\mathbf{e}_2$ are the base vectors. The Bloch–Floquet boundary conditions should be imposed on the unit cell, and the periodic displacement fields and the periodic stress fields can be represented as $\mathbf{u}(\mathbf{x} + \mathbf{r}) = \mathbf{u}(\mathbf{x})\exp(\mathbf{k}\cdot\mathbf{r})$ and $\boldsymbol{\sigma}(\mathbf{x} + \mathbf{r}) = \boldsymbol{\sigma}(\mathbf{x})\exp(\mathbf{k}\cdot\mathbf{r})$, respectively, where $\mathbf{x} = x_1\mathbf{e}_1 + x_2\mathbf{e}_2$ is the position vector of the point in the unit cell and the wave vector is introduced as $\mathbf{k} = k_1\mathbf{e}_1 + k_2\mathbf{e}_2$. Specifically, for the one-dimensional (1D) periodic structure and the corresponding unit cell in Figure 2, we have

$$u_i(x_2 = 2h_0) = \exp(i2k_2h_0)u_i(x_2 = 0), \sigma_{2i}(x_2 = 2h_0) = \exp(i2k_2h_0)\sigma_{2i}(x_2 = 0). \tag{5}$$

3. SEM

The SEM is taken to simulate the guided waves propagating in the stack of elastic layers by considering the interfacial delaminations in the frequency domain. In addition, the SEM is extended to obtain the dispersion curves for the unit cells with or without interfacial delaminations imposed by the Bloch–Floquet boundary conditions.

The weak form of the equations of motion (1) can be obtained by employing the Galerkin method as [28]

$$\iint_S \left(\sigma_{ij,j} + b_i + \rho\omega^2 u_i\right)w_i dx_1 dx_2 = 0, \tag{6}$$

where w_i ($i = 1, 2$) are the test functions, S represents the area of the element, and the repeated subscripts denote the summation.

The integration by parts and the application of Green's formula to equation (6) yield

$$\iint_S \sigma_{ij}w_{i,j} dx_1 dx_2 = \iint_S \left(\rho\omega^2 u_i + b_i\right)w_i dx_1 dx_2 + \oint_R w_i f_i dl, \tag{7}$$

where $f_i = \sigma_{ij}n_j$ is the component of the traction vector, with n_j being the component of the outward unit normal vector of the boundary R of the domain S. The body forces will not be considered in this paper by setting $b_i = 0$.

The domain can be discretized by a number of elements like the conventional FEM. And the displacement components in each element can be approximated by the interpolation or shape functions as

$$u_i^e = \sum_{I=1}^{N} u_i^{eI} \psi_I^e(x_1, x_2),$$
(8)

where N is the number of the nodes, u_i^{eI} is the displacement component of the Ith node in the eth element, and $\psi_I^e(x_1, x_2)$ is the interpolation or shape function for the 2D problem.

In each element, the Lagrange polynomials are used to approximate the displacement field using the spectral interpolation nodes. The Gauss–Lobatto–Legendre basis functions are adopted, whose 1D pth order form is given by Pozrikidis [30]

$$\chi_i^{(p)}(\xi) = \frac{-1}{p(p+1)L_p(\xi_i)} \frac{(1-\xi^2)L_p^{'}(\xi)}{\xi - \xi_i},$$
(9)

where $\xi \in [-1, 1]$, $L_p(\xi_i)$ and $L_p^{'}(\xi)$ are the pth order Legendre polynomial and its derivative, respectively, and ξ_i ($i = 0, 1 \cdots p$) are the roots of the equation $(1 - \xi^2)L_p^{'}(\xi) = 0$ and are called the spectral nodes. The interpolation polynomials for the 2D case can be represented by the direct product of two 1D Gauss–Lobatto–Legendre basis functions as

$$\psi_I^e(\xi, \eta) = \chi_i^{(p)}(\xi)\chi_j^{(p)}(\eta),$$
(10)

where I is the compound index with a convection relation to the indexes i and j. The global coordinates (x_1, x_2) for the nodes in the eth element and the local coordinates (ξ, η) can be related by $x_1 = e_1^e + l_1^e \xi$ and $x_2 = e_2^e + l_2^e \eta$, where (e_1^e, e_2^e) are the coordinates of the central point of the eth element, l_1^e and l_2^e are the length and the width of the element, respectively.

The same interpolation functions ψ_I^e are also employed to approximate the test functions as

$$w_i^e = \sum_{I=1}^{N} \delta u_i^{eI} \psi_I^e(x_1, x_2),$$
(11)

where δu_i^{eI} is the virtual displacement component.

The expressions of the discretized form of the components of the stress tensor can be obtained by substituting equation (8) into equation (2). Then, in view of these expressions and equations (8)–(11), the discretized form of the weak form of the equations of motion (7) can be achieved. Following the similar procedure as in the conventional FEM, the matrix form of the discretized algebraic equations can be written as

$$\left(\mathbf{K}^e - \omega^2 \mathbf{M}^e\right)\mathbf{u}^e = \mathbf{F}^e,$$
(12)

where

$$\mathbf{K}^e = \begin{bmatrix} \mathbf{K}^{11} & \mathbf{K}^{12} \\ \mathbf{K}^{21} & \mathbf{K}^{22} \end{bmatrix}, \mathbf{M}^e = \begin{bmatrix} \mathbf{M}^{11} & \mathbf{0} \\ \mathbf{0} & \mathbf{M}^{22} \end{bmatrix}, \mathbf{u}^e = \begin{bmatrix} \mathbf{u}_1^e \\ \mathbf{u}_2^e \end{bmatrix}, \mathbf{F}^e = \begin{bmatrix} \mathbf{F}_1^e \\ \mathbf{F}_2^e \end{bmatrix},$$
(13)

where $\mathbf{u}_1^e$ and $\mathbf{u}_2^e$ represent the vectors of the nodal displacements in the eth element, which can be expressed as

$$\mathbf{u}_1^e = \left\{ u_1^1 \quad u_1^2 \quad u_1^3 \quad \cdots \quad u_1^N \right\}^T,$$
$$\mathbf{u}_2^e = \left\{ u_2^1 \quad u_2^2 \quad u_2^3 \quad \cdots \quad u_2^N \right\}^T,$$
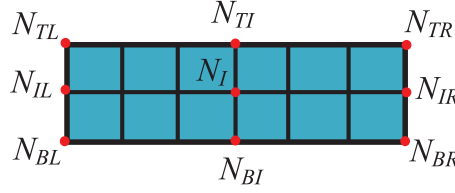(14)

Figure 3. Schematic diagram of the SEM mesh.

$\mathbf{F}_1^e$ and $\mathbf{F}_2^e$ represent the vectors of the nodal forces along the x_1- and x_2-axes, respectively, in the eth element, which are given by

$$\mathbf{F}_i^e = \oint_{L^e} f_i^e \{\, \psi_1^e \quad \psi_2^e \quad \cdots \quad \psi_N^e \,\}^T \left(-n_3 l_1^e d\xi + n_1 l_3^e d\eta\right), (i = 1, 2), \tag{15}$$

where L^e represents the boundary of the domain of the eth element. The components of the stiffness matrix can be given by

$$K_{I'I}^{11} = \frac{E(1-\nu)}{(1+\nu)(1-2\nu)} I_{I'I}^{11} + \frac{E}{2(1+\nu)} I_{I'I}^{22}, K_{I'I}^{12} = \frac{E\nu}{(1+\nu)(1-2\nu)} I_{I'I}^{12} + \frac{E}{2(1+\nu)} I_{I'I}^{21}$$
$$K_{I'I}^{21} = \frac{E}{2(1+\nu)} I_{I'I}^{12} + \frac{E\nu}{(1+\nu)(1-2\nu)} I_{I'I}^{21}, K_{I'I}^{22} = \frac{E}{2(1+\nu)} I_{I'I}^{11} + \frac{E(1-\nu)}{(1+\nu)(1-2\nu)} I_{I'I}^{22}, \tag{16}$$

where

$$I_{I'I}^{11} = \iint_{S^e} \frac{1}{(l_1^e)^2} \frac{\partial \psi_{I'}^e}{\partial \xi} \frac{\partial \psi_I^e}{\partial \xi} \det(\mathbf{J}) d\xi d\eta, I_{I'I}^{22} = \iint_{S^e} \frac{1}{(l_2^e)^2} \frac{\partial \psi_{I'}^e}{\partial \eta} \frac{\partial \psi_I^e}{\partial \eta} \det(\mathbf{J}) d\xi d\eta,$$
$$I_{I'I}^{21} = \iint_{S^e} \frac{1}{l_1^e} \frac{1}{l_2^e} \frac{\partial \psi_{I'}^e}{\partial \eta} \frac{\partial \psi_I^e}{\partial \xi} \det(\mathbf{J}) d\xi d\eta, I_{I'I}^{12} = \iint_{S^e} \frac{1}{l_1^e} \frac{1}{l_2^e} \frac{\partial \psi_{I'}^e}{\partial \xi} \frac{\partial \psi_I^e}{\partial \eta} \det(\mathbf{J}) d\xi d\eta. \tag{17}$$

The two nonzero sub-matrices of the mass matrix have the same expression, which can be represented by

$$M_{II'} = \iint_{S^e} \rho \psi_{I'}^e \psi_I^e \det(\mathbf{J}) d\xi d\eta. \tag{18}$$

Both the stiffness matrix and the mass matrix are $2N \times 2N$ symmetric matrices and independent of the frequency.

The global system of linear algebraic equations can be obtained by the same procedure of FEM as $(\mathbf{K} - \omega^2 \mathbf{M})\mathbf{u} = \mathbf{F}$ and the conventional boundary value problem can be solved in a similar way. In the following part, the discretized form of the Bloch–Floquet boundary conditions in equation (5) is derived for the unit cell in the infinite stack of periodic elastic layers, which can be expressed by

$$\mathbf{D}_N^T = e^{i2k_2h_0} \mathbf{D}_N^B, \tag{19}$$

where $\mathbf{D}_N^T = \{\, u_1^T \quad u_2^T \quad \sigma_{12}^T \quad \sigma_{22}^T \,\}$ and $\mathbf{D}_N^B = \{\, u_1^B \quad u_2^B \quad \sigma_{12}^B \quad \sigma_{22}^B \,\}$. Referring to Figure 3, the letters in the subscripts represent the locations of the nodes in this part, i.e., "I" represents the internal nodes, "T" and "B" represent the nodes on the top and bottom lines, respectively, and "R" and "L" represent the nodes on the right and left sides of the unit cell, respectively.

In consideration of the discretized form of the Bloch–Floquet boundary conditions (equation (19)), the displacement vector and the force vector of the unit cell can be reduced to

$$
\begin{Bmatrix} \mathbf{u}_I \\ \mathbf{u}_{IL} \\ \mathbf{u}_{IR} \\ \mathbf{u}_{BL} \\ \mathbf{u}_{BI} \\ \mathbf{u}_{BR} \\ \mathbf{u}_{TL} \\ \mathbf{u}_{TI} \\ \mathbf{u}_{TR} \end{Bmatrix} = \begin{Bmatrix} \mathbf{u}_I \\ \mathbf{u}_{IL} \\ \mathbf{u}_{IR} \\ \mathbf{u}_{BL} \\ \mathbf{u}_{BI} \\ \mathbf{u}_{BR} \\ e^{i2k_2h_0}\mathbf{u}_{BL} \\ e^{i2k_2h_0}\mathbf{u}_{BI} \\ e^{i2k_2h_0}\mathbf{u}_{BR} \end{Bmatrix} = \mathbf{A}_u \begin{Bmatrix} \mathbf{u}_I \\ \mathbf{u}_{IL} \\ \mathbf{u}_{IR} \\ \mathbf{u}_{BL} \\ \mathbf{u}_{BI} \\ \mathbf{u}_{BR} \end{Bmatrix} = \mathbf{A}_u \bar{\mathbf{u}}, \quad \begin{Bmatrix} \mathbf{F}_I \\ \mathbf{F}_{IL} \\ \mathbf{F}_{IR} \\ \mathbf{F}_{BL} \\ \mathbf{F}_{BI} \\ \mathbf{F}_{BR} \\ \mathbf{F}_{TL} \\ \mathbf{F}_{TI} \\ \mathbf{F}_{TR} \end{Bmatrix} = \begin{Bmatrix} \mathbf{0} \\ \mathbf{0} \\ \mathbf{0} \\ \mathbf{F}_{BL} \\ \mathbf{F}_{BI} \\ \mathbf{F}_{BR} \\ -e^{i2k_2h_0}\mathbf{F}_{BL} \\ -e^{i2k_2h_0}\mathbf{F}_{BI} \\ -e^{i2k_2h_0}\mathbf{F}_{BR} \end{Bmatrix},
\tag{20}
$$

where $\bar{\mathbf{u}}$ represents the displacement vector of the independent nodes. For the force vector, the condition of the zero traction on the left and the right boundaries is considered and the relation $\mathbf{f}_T = \boldsymbol{\sigma}_T = e^{i2k_2h_0}\boldsymbol{\sigma}_B = -e^{i2k_2h_0}\mathbf{f}_B$ is used, which is derived based on the expression of the traction $f_i = \sigma_{ij}n_j$.

In view of equation (20), the global system equation can be rewritten as

$$
(\mathbf{K} - \omega^2\mathbf{M})\mathbf{A}_u\bar{\mathbf{u}} = \mathbf{F}.
\tag{21}
$$

Furtherly, multiplying the both sides of equation (21) by $\mathbf{A}_f$ we get the reduced form of the system equation as

$$
(\bar{\mathbf{K}} - \omega^2\bar{\mathbf{M}})\bar{\mathbf{u}} = \mathbf{A}_f\mathbf{F} = \mathbf{0},
\tag{22}
$$

where

$$
\bar{\mathbf{K}} = \mathbf{A}_f\mathbf{K}\mathbf{A}_u, \bar{\mathbf{M}} = \mathbf{A}_f\mathbf{M}\mathbf{A}_u,
\tag{23}
$$

and $\mathbf{A}_f$ can be calculated as

$$
\mathbf{A}_f = \begin{bmatrix} \mathbf{I} & \mathbf{0} & \mathbf{0} & \mathbf{0} & \mathbf{0} & \mathbf{0} & \mathbf{0} & \mathbf{0} & \mathbf{0} \\ \mathbf{0} & \mathbf{I} & \mathbf{0} & \mathbf{0} & \mathbf{0} & \mathbf{0} & \mathbf{0} & \mathbf{0} & \mathbf{0} \\ \mathbf{0} & \mathbf{0} & \mathbf{I} & \mathbf{0} & \mathbf{0} & \mathbf{0} & \mathbf{0} & \mathbf{0} & \mathbf{0} \\ \mathbf{0} & \mathbf{0} & \mathbf{0} & e^{i2k_2h_0}\mathbf{I} & \mathbf{0} & \mathbf{0} & \mathbf{I} & \mathbf{0} & \mathbf{0} \\ \mathbf{0} & \mathbf{0} & \mathbf{0} & \mathbf{0} & e^{i2k_2h_0}\mathbf{I} & \mathbf{0} & \mathbf{0} & \mathbf{I} & \mathbf{0} \\ \mathbf{0} & \mathbf{0} & \mathbf{0} & \mathbf{0} & \mathbf{0} & e^{i2k_2h_0}\mathbf{I} & \mathbf{0} & \mathbf{0} & \mathbf{I} \end{bmatrix},
\tag{24}
$$

where $\mathbf{I}$ is an identity matrix.

For the nontrivial solutions to equation (22), the determinant of the coefficient matrix must be zero as follows

$$
\left| \bar{\mathbf{K}} - \omega^2\bar{\mathbf{M}} \right| = 0.
\tag{25}
$$

The dispersion relation of the guided waves in the unit cell imposed by the Bloch–Floquet boundary conditions can be calculated from equation (25).

4. Numerical results and discussions

In this section, the dispersion curves for the unit cell imposed by the Bloch–Floquet boundary conditions and the transmission spectra for the finite stack of periodic elastic layers are both calculated. The partial band-gaps of the guided waves propagating in the blocking zone are much critical for the realization of unidirectional propagation of the guided waves, in which the propagation of the guided waves with the specified wave mode is prohibited. Thus, the corresponding dispersion curves are firstly calculated, which are shown in Figures 4(a)–(c) for the blocking zone with no interfacial delamination, the array of symmetric central and side interfacial delaminations, respectively. The dispersion curves are also calculated by COMSOL Multiphysics to verify the computational codes in this paper. For the
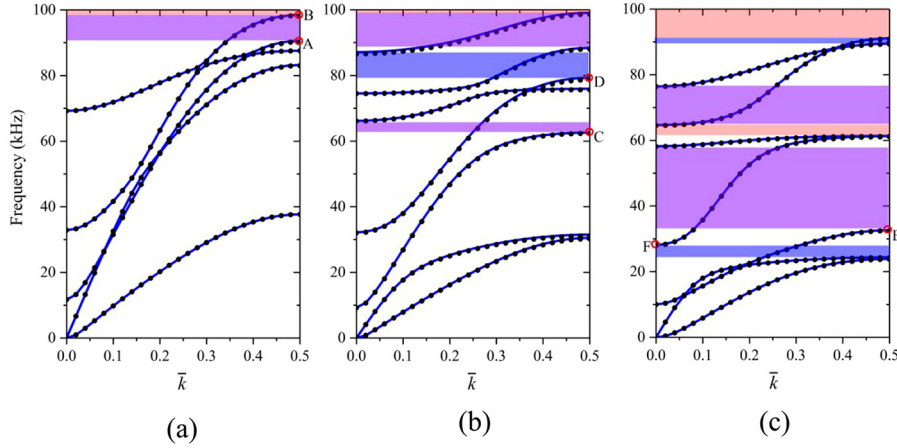
Figure 4. The band-gaps of the guided waves propagating in the blocking zone without interfacial delamination (a), and with the array of symmetric (b) central and (c) side interfacial delaminations, respectively. The black dots represent the results calculated by COMSOL Multiphysics. The dimensionless quantity $\bar{k}$ is defined as $2h_0$/wavelength. The blue, the purple, and the red shadows represent the partial band-gaps of symmetric and antisymmetric guided waves and the complete band-gaps, respectively.

blocking zone with no interfacial delamination, the partial band-gap of symmetric guided wave intersects with the partial band-gap of antisymmetric guided wave, which produces the complete band-gap where all the guided wave propagation is prohibited. Thus, the guided waves cannot propagate along both directions in this complete band-gap. However, in the frequency range [0–100 kHz], there is no partial band-gap of symmetric guided wave for the blocking zone with no interfacial delamination, which is the limitation of this structure.

To solve this problem, the array of symmetric interfacial delaminations can be inserted into the blocking zone, which will not lead to wave mode transformation. The illustration of the array of the symmetric interfacial delaminations can be found in Figure 2(b) and the corresponding boundary conditions are described by equation (4). It is uncovered from Figures 4(b) and 4(c) that the array of symmetric interfacial delaminations is able to produce separated partial band-gaps of both symmetric and antisymmetric guided waves in the low-frequency region. Specifically, two extra separated partial band-gaps are produced by the array of the symmetric central interfacial delaminations (see Figure 4(b)), and three extra separated partial band-gaps are induced by the array of the symmetric side interfacial delaminations (see Figure 4(c)). The mechanism behind this phenomenon may be revealed through the analysis of some wave mode shapes corresponding to the nodes on the boundaries of the band-gaps, see Figure 5. For example, comparing the wave mode shapes C–F with the wave mode shapes A and B, it can be found that the large deformations happen around the central and the side interfacial delamination since these band-gaps are generated by the resonance of the elastic layers lying between the two neighboring interfacial delaminations [28]. Thus, the resonance frequencies can be predicted by the beam fixed at both sides for the central delamination and by the cantilever beam for the side delamination. In addition, the wave mode shape F is a special case, which is the only lowest order wave mode for the structure. Through the comparison of Figure 4(c) with Figures 4(a) and 4(b), it is found that this partial band-gap of the lowest symmetric guided wave can only be opened by the array of the symmetric side delaminations. The possible mechanism behind this phenomenon is that the natural frequency of the cantilever beam-like structure formed by the debonded layer between two neighboring side delaminations is lower than the natural frequency of the corresponding beam-like structure fixed on both sides built by the debonded layer between two neighboring central delaminations.

In addition, we also find that the partial band-gaps of the antisymmetric guided waves are wider than the partial band-gaps (see Figure 4). The models presented in Figure 2 can be viewed as beam-like structures if we rotate them by 90 degrees, and the interfacial delaminations can be considered as a reduction of the height of a beam. Thus, the symmetric guided wave can be regarded as the longitudinal wave, while the antisymmetric guided wave can be regarded as the bending or flexural wave, which depend on the tensile stiffness $EA = (Et)w$ and the bending stiffness $EI = (Et/12)w^3$, respectively, where t is the
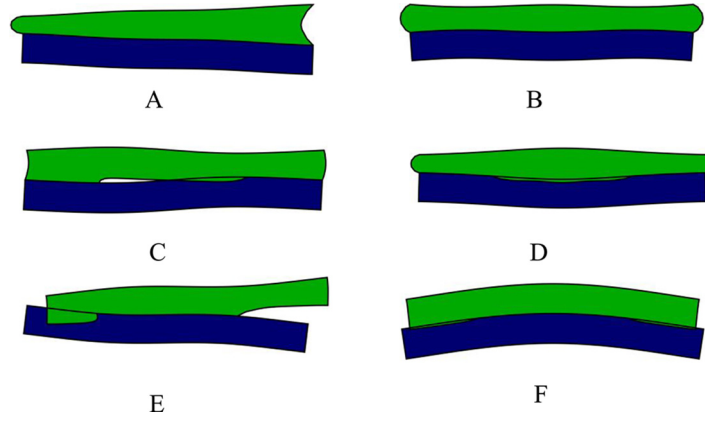
Figure 5. The wave mode shapes (A)–(F) corresponding to the points A–F in Figure 4.

width of the beam and the thickness of the elastic layer w can be regarded as the height of the beam. Since the tensile stiffness is proportional to w and the bending stiffness is dependent on w^3, the variation of the bending stiffness is stronger than the variation of the tensile stiffness for the same reduction of the height w of the beam induced by the interfacial delaminations, which may lead to more partial band-gaps of the antisymmetric guided waves. Hence, we can conclude that the unidirectional propagation of the antisymmetric guided waves can be more likely generated by inserting the array of the interfacial delaminations in the low-frequency range.

To verify the above analysis related to the band-gaps, the transmission spectra are calculated. The transmission of the guided waves over the whole structures along the positive and the negative directions of x_2-axis is analyzed, respectively. The symmetric and the antisymmetric excitations are considered separately. The symmetric displacement excitation can be denoted by $u_1 = 0$ and $u_2 = v_0$ and the antisymmetric displacement excitation can be denoted by $u_1 = u_0$ and $u_2 = 0$. If the excitation is put on the bottom line of the structure, the receiver should be put on the top line, and vice versa (see Figure 1). The guided waves would propagate along the positive and the negative directions, respectively, for the above two cases. The transmission of the guided waves is defined as

$$\text{Transmission} = 20\log_{10}\left(\frac{\int_{l_R}\sqrt{u_1^2 + u_2^2}dx_2}{|D|w}\right) \approx 20\log_{10}\left(\frac{\sum_{i=1}^{\bar{N}}\sqrt{u_1^i + u_2^i}}{|D|\bar{N}}\right), \tag{26}$$

where u_1 and u_2 are the displacement components of the node on the line of receiver, D represents the total displacement of the node on the line of excitation with the length w, i.e., v_0 for the symmetric excitation and u_0 for the antisymmetric excitation, and $\bar{N}$ is the number of the nodes on the line of receiver or excitation.

The transmission spectra of the guided waves propagating in the stack of periodic elastic layers without interfacial delamination in the blocking zone (see Figure 2(a)) are presented in Figure 6. The spatial inversion symmetry of the stack is broken due to the insertion of the array of asymmetric interfacial delaminations. However, for the symmetric excitation, there is no frequency range where the unidirectional transmission of the guided wave exists (see Figure 6(a)). For the antisymmetric excitation, the unidirectional propagation of the guided waves is realized in the frequency range [90.6–98.5 kHz]. For example, the guided waves excited at 94 kHz from the bottom line attenuate very quickly (see Figure 7(a)), while the guided waves excited from the top line at the same frequency can transmit over the whole structure to the bottom line (see Figure 7(b)). The key point behind this phenomenon is that the symmetric guided waves can be generated when the antisymmetric guided waves pass through the asymmetric structures or the asymmetric interfacial delaminations, i.e., the transformation zone. Thus, both of the symmetric and the antisymmetric guided waves exist in the transformation zone at the beginning.
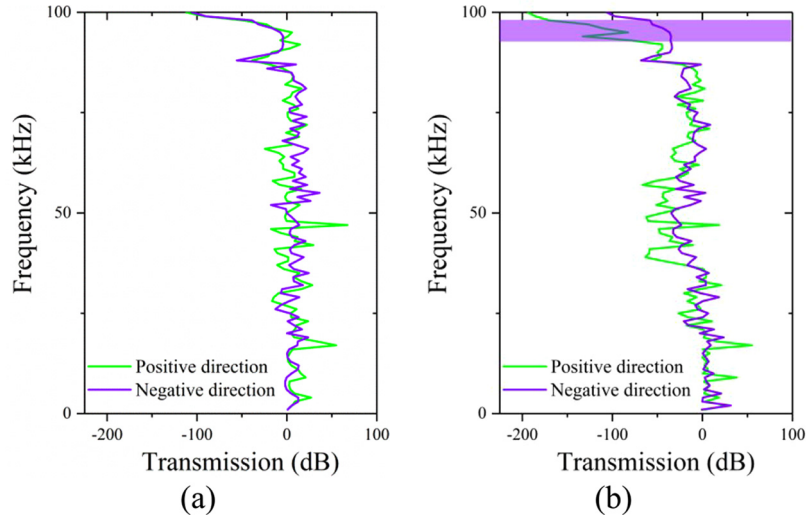
Figure 6. Transmission spectra of the guided waves propagating along the positive and the negative directions in the stack of periodic elastic layers without interfacial delamination in the blocking zone (see Figure 2a) under (a) the symmetric excitation and (b) the antisymmetric excitation, respectively.
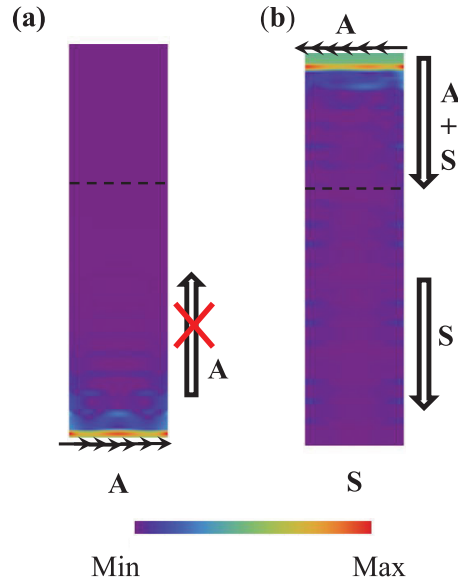

Figure 7. Displacement fields in the stack of periodic elastic layers without interfacial delamination in the blocking zone under the antisymmetric excitations (a) on the bottom side and (b) on the top side at 94 kHz. The dotted lines denote the interfaces between the transformation zones and the blocking zones.

Then, the antisymmetric guided waves disappear quickly after they enter the blocking zone within the partial band-gap of antisymmetric guided waves. Finally, only the guided waves with the symmetric wave mode can transmit over the blocking zone. However, the shortcoming is that the unidirectional transmission of the symmetric guided waves is relatively low (see Figure 6(b) or 7(b)).

The transmission spectra of the guided waves propagating in the stack of periodic elastic layers with the array of the symmetric central interfacial delaminations in the blocking zone (see Figure 2(b)) are presented in Figure 8. Due to the insertion of the array of the symmetric central interfacial delaminations into the blocking zone, the partial band-gap of symmetric guided wave appears in the frequency range [79.2–87.2 kHz], see Figure 8(a), which agrees with the analysis for the dispersion curves in Figure
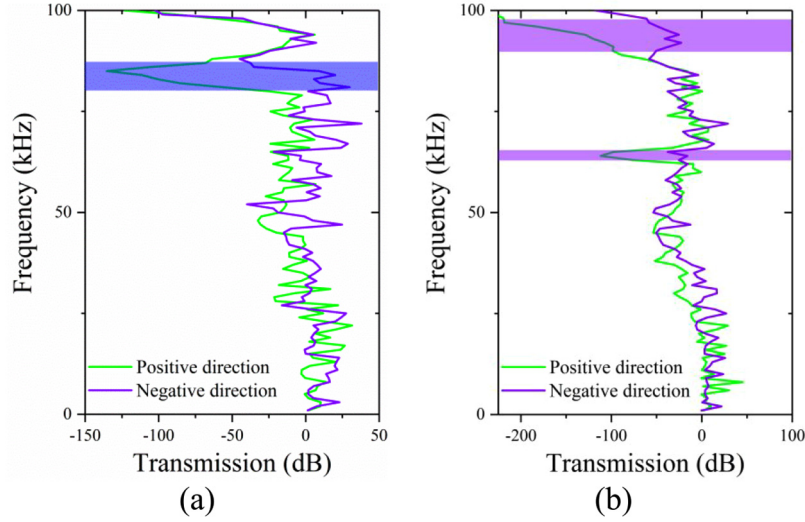
Figure 8. Transmission spectra of the guided waves propagating along the positive and the negative directions in the stack of periodic elastic layers with the array of the symmetric central interfacial delaminations in the blocking zone (see Figure 2(b)) under (a) the symmetric excitation and (b) the antisymmetric excitation, respectively.
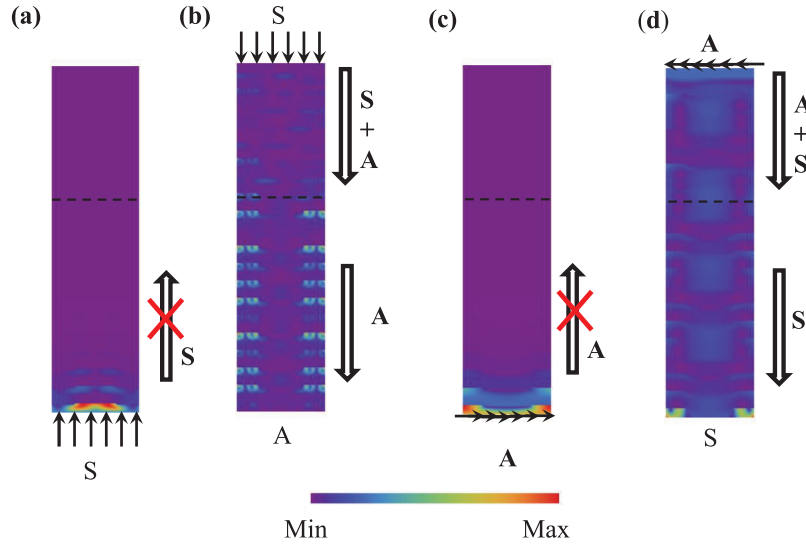

Figure 9. Displacement fields in the stack of periodic elastic layers with the array of the symmetric central interfacial delaminations in the blocking zone under the symmetric excitations (a) on the bottom line and (b) on the top line at 85 kHz, and under the antisymmetric excitations (c) on the bottom line and (d) on the top line at 64 kHz. The dotted lines denote the interfaces between the transformation zones and the blocking zones.

4(b). Thus, the unidirectional propagation is possible for the symmetric excitation (see Figures 9(a) and 9(b)). The symmetric guided waves at 85 kHz excited on the bottom line cannot propagate along the positive direction of x_2-axis over the blocking zone within the partial band-gap of symmetric guided wave (see Figure 9(a)). However, the guided waves induced by the same excitation propagating from the top line can transmit over the blocking zone successfully due to the generation of the antisymmetric guided waves in the transformation zone. And the antisymmetric guided waves can pass through the blocking zone since the partial band-gaps of the symmetric and the antisymmetric guided waves are separated. For the antisymmetric excitation, there are two frequency ranges [62.7–65.5 kHz] and [88.8–98.9 kHz], in which the unidirectional transmission of the guided waves can be realized. For example,
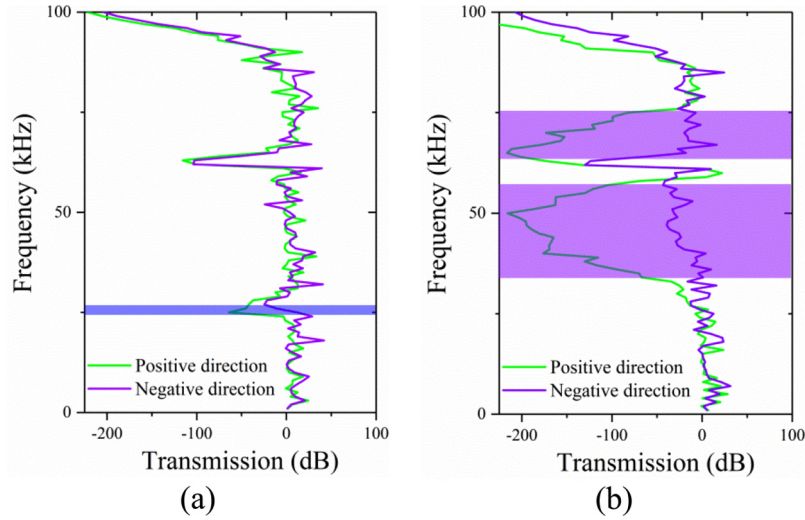
Figure 10. Transmission spectra of the guided waves propagating along the positive and the negative directions in the stack of periodic elastic layers with the array of the symmetric side interfacial delaminations in the blocking zone (see Figure 2(c)) under (a) the symmetric excitation and (b) the antisymmetric excitation, respectively.

Figures 9(c) and (9d) show that the guided waves excited by the antisymmetric source at 64 kHz can only propagate from the top line to the bottom line.

The transmission spectra of the guided waves propagating in the stack of periodic elastic layers with the array of the symmetric side interfacial delaminations in the blocking zone are presented in Figure 10. From the transmission spectra, the unidirectional transmission of guided waves are obviously observed in the frequency range [24.5–27.7 kHz] for the symmetric excitation and the frequency ranges [33.1–57.7 kHz] and [65.2–76.6 kHz] for the antisymmetric excitation. The partial band-gap [89.1–91.1 kHz] of symmetric guided waves cannot be observed obviously from Figure 10(a), which, however, can be found from the dispersion curves in Figure 4(c). The reason is that the attenuation of the symmetric guided waves is small when they pass through the blocking zone due to the finite number of unit cells. In addition, this partial band-gap is very close to the complete band-gap, which leads to a low unidirectional transmission. As examples, the unidirectional propagations of the guided waves excited symmetrically at 25 kHz and antisymmetrically at 40 kHz are both shown in Figure 11.

The advantages of the array of the symmetric central and side interfacial delaminations in the blocking zones can be uncovered from the comparison of the dispersion curves in Figures 4(a)–4(c). The array of the symmetric central interfacial delaminations can generate a larger partial band-gap of symmetric guided waves and realize the relatively high unidirectional transmission of the guided waves. The array of the symmetric side interfacial delaminations can give rise to a partial band-gap of the lowest symmetric guided wave and induce more and wider partial band-gaps of antisymmetric guided waves in the low-frequency range.

5. Concluding remarks

The unidirectional propagation of guided waves is theoretically explored in the stack of periodic elastic layers with an array of interfacial delaminations. The whole structure consists of two parts and the concept of wave mode transformation is adopted. The array of asymmetric interfacial delaminations is intentionally inserted into the top part of the finite stack to change the mode of the guided wave. We call this top part the transformation zone. The bottom part composed of the periodic elastic layers can be used to block the propagation of the guided waves with the specified mode within the partial band-gaps. Thus, the separated partial band-gaps are much crucial for the realization of the unidirectional propagation of the guided waves. The bottom part is called the blocking zone. However, the shortcoming of the blocking zone without interfacial delamination is that the partial band-gap of symmetric guided waves
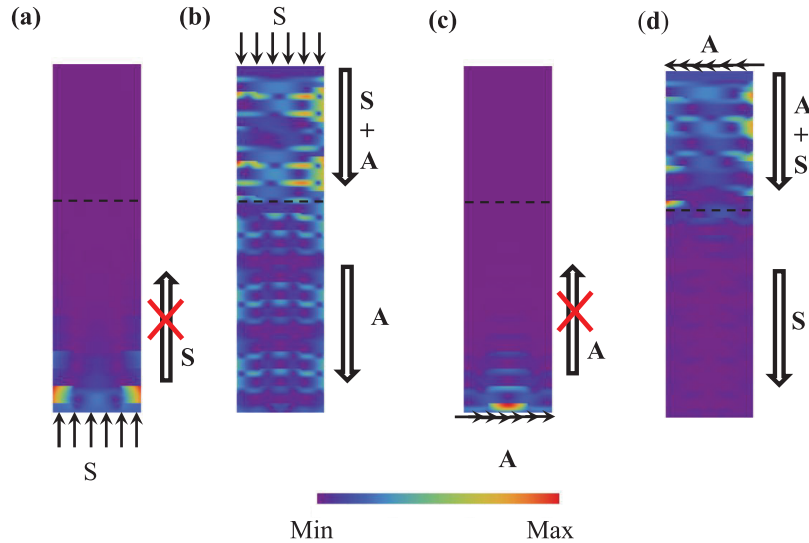
Figure 11. Displacement fields in the stack of periodic elastic layers with the array of the symmetric side interfacial delaminations in the blocking zone under the symmetric excitations (a) on the bottom line and (b) on the top line at 25 kHz, and under the antisymmetric excitations (c) on the bottom line and (d) on the top line at 40 kHz. The dotted lines denote the interfaces between the transformation zones and the blocking zones.

does not exist in the low-frequency range. To solve this problem, the array of symmetric central or side interfacial delaminations is inserted into the blocking zone to gain more band-gaps, especially the separated partial band-gaps.

The transmission spectra of the guided waves propagating in the finite stack of periodic elastic layers with interfacial delaminations and the dispersion curves for the unit cell imposed by the Bloch–Floquet boundary conditions are both calculated by the SEM. Then, we numerically confirm that the symmetric (antisymmetric) guided waves excited from the bottom side cannot propagate over this structure in the partial band-gaps of symmetric (antisymmetric) guided waves, the same guided waves, however, excited on the top side can transmit over this structure successfully with the changed mode. In addition, the introduction of the array of the symmetric central or side interfacial delaminations into the blocking zone can efficiently enlarge the frequency ranges where the unidirectional transmission of the guided waves is allowed. Through the comparison of the partial band-gaps and the wave transmittance, the advantages of the array of the symmetric central and side interfacial delaminations in the blocking zones are uncovered for the symmetric and the antisymmetric excitations, respectively.

The proposed structure may have potential applications in the field of wave propagation isolation and information processing. In addition, we suggest a new concept to control the wave propagation in phononic crystals using interfacial delaminations or cracks.

ORCID iDs

Mikhail V Golub https://orcid.org/0000-0003-4927-9623
Weiqiu Chen https://orcid.org/0000-0003-0655-3303

References

[1] Ke, M, Liu, Z, Qiu, C, et al. Negative-refraction imaging with two-dimensional phononic crystals. *Phys Rev B* 2005; 72: 064306.

[2] Wang, J, Huang, Y, Chen, W, et al. Abnormal wave propagation behaviors in two-dimensional mass–spring structures with nonlocal effect. *Math Mech Solids* 2019; 24: 3632–3643.

[3] Zhang, S, Yin, L, and Fang, N. Focusing ultrasound with an acoustic metamaterial network. *Phys Rev Lett* 2009; 102: 194301.

[4] Cummer, SA, Popa, BI, Schurig, D, et al. Scattering theory derivation of a 3D acoustic cloaking shell. *Phys Rev Lett* 2008; 100: 024301.

[5] Rostami-Dogolsara, B, Moravvej-Farshi, MK, and Nazari, F. Acoustic add-drop filters based on phononic crystal ring resonators. *Phys Rev B* 2016; 93: 014304.

[6] Vasseur, JO, Deymier, PA, Djafari-Rouhani, B, et al. Absolute forbidden bands and waveguiding in two-dimensional phononic crystal plates. *Phys Rev B* 2008; 77: 085415.

[7] Zhou, X, Assouar, MB, and Oudich, M. Acoustic superfocusing by solid phononic crystals. *Appl Phys Lett* 2014; 105: 233506.

[8] Zou, Q, Liu, W, Yu, T, et al. Decoupling of multiple coupled phononic crystal waveguides: application to acoustic demultiplexing. *J Phys D: Appl Phys* 2017; 50: 125102.

[9] Cummer, SA, Christensen, J, and Alù, A. Controlling sound with acoustic metamaterials. *Nat Mater Rev* 2016; 1: 1–13.

[10] Sugino, C, Ruzzene, M, and Erturk, A. Nonreciprocal piezoelectric metamaterial framework and circuit strategies. *Phys Rev B* 2020; 102: 014304.

[11] Liang, B, Yuan, B, and Cheng, JC. Acoustic diode: rectification of acoustic energy flux in one-dimensional systems. *Phys Rev Lett* 2009; 103: 104301.

[12] Liang, B, Guo, XS, Tu, J, et al. An acoustic rectifier. *Nat Mater* 2010; 9: 989–992.

[13] Li, XF, Ni, X, Feng, L, et al. Tunable unidirectional sound propagation through a sonic-crystal-based acoustic diode. *Phys Rev Lett* 2011; 106: 084301.

[14] Trainiti, G, and Ruzzene, M. Non-reciprocal elastic wave propagation in spatiotemporal periodic structures. *New J Phys* 2016; 18: 083047.

[15] Nassar, H, Xu, XC, Norris, AN, et al. Modulated phononic crystals: non-reciprocal wave propagation and Willis materials. *J Mech Phys Solids* 2017; 101: 10–29.

[16] Nassar, H, Chen, H, Norris, AN, et al. Non-reciprocal wave propagation in modulated elastic metamaterials. *Proc. Math. Phys. Eng. Sci* 2017; 473: 20170188.

[17] Zhu, X, Zou, X, Liang, B, et al. One-way mode transmission in one-dimensional phononic crystal plates. *J Appl Phys* 2010; 108: 124909.

[18] Zou, XY, Liang, B, Yuan, Y, et al. Controllable acoustic rectification in one-dimensional piezoelectric composite plates. *J Appl Phys* 2013; 114: 164504.

[19] Feng, F, Shen, Z, and Shen, J. Edge waves in a 3D plate: two solutions based on plate mode matching. *Math Mech Solids* 2017; 22: 2065–2074.

[20] Song, Z, and Dai, HH. On a consistent dynamic finite-strain plate theory and its linearization. *J Elast* 2016; 125: 149–183.

[21] Wang, Y, Li, Z, Chen, W, et al. Free vibration and active control of pre-stretched multilayered electroactive plates. *Int J Solids Struct* 2019; 180: 108–124.

[22] Gao, L, Wang, J, Zhong, Z, et al. An analysis of surface acoustic wave propagation in functionally graded plates with homotopy analysis method. *Acta Mech* 2009; 208: 249–258.

[23] Gao, L, Wang, J, Zhong, Z, et al. An exact analysis of surface acoustic waves in a plate of functionally graded materials. *IEEE T Ultrason Ferroelect Freq Contr* 2009; 52: 2693–2700.

[24] Gao, L, Wang, J, Zhong, Z, et al. An analysis of surface acoustic wave propagation in a plate of functionally graded materials with a layered model. *Sci China Ser G* 2008; 51: 165–175.

[25] Achenbach, JD. *Reciprocity in elastodynamics*. Cambridge: Cambridge University Press, 2003, p. 200.

[26] Chen, Y, Wu, B, Su, Y, et al. Tunable two-way unidirectional acoustic diodes: design and simulation. *J Appl Mech* 2019; 86: 031010.

[27] Chen, Y, Huang, Y, Lü, C, et al. A two-way unidirectional narrow-band acoustic filter realized by a graded phononic crystal. *J Appl Mech* 2017; 84.

[28] Wang, Y, Perras, E, Golub, MV, et al. Manipulation of the guided wave propagation in multilayered phononic plates by introducing interface delaminations. *Eur J Mech A Solids* 2021; 88: 104266.

[29] Kim, Y, Ha, S, and Chang, FK. Time-domain spectral element method for built-in piezoelectric-actuator-induced Lamb wave propagation analysis. *AIAA J* 2008; 46: 591–600.

[30] Pozrikidis, C. *Introduction to finite and spectral element methods using MATLAB*. 2nd ed. Boca Raton, FL: CRC Press, 2014, p. 155.